Mon. Not. R. Astron. Soc. **341,** 1349–1359 (2003)

The planetary nebula K 1-2 and its binary central star VW Pyx

K. M. Exter,[1]★ D. L. Pollacco[1] and S. A. Bell[2]

[1]*APS Division, Department of Pure and Applied Physics, Queen's University Belfast, Belfast BT7 1NN*
[2]*HM Nautical Almanac Office, Space Science and Technology Department, Rutherford Appleton Laboratory, Chilton, Didcot OX11 0QX*

Accepted 2003 February 6. Received 2003 February 6; in original form 2002 December 16

ABSTRACT

New data are presented of the post-common-envelope binary VW Pyx and its associated planetary nebula (PN), K 1-2. The central star is found to be a single-lined (and possibly double-lined) spectroscopic binary and is a good candidate for a system in which the main-sequence secondary star is more massive than the subdwarf primary star. The old PN has a high excitation level and a measured electron temperature, $T_{\rm O} \sim 17\,000$ K for an assumed $\log n_{\rm e} = 2.7$ cm^{-3}. The so-called 'jets' are found to be lower-ionization regions with $T_{\rm N} \sim 11\,000$ K and $T_{\rm O} \sim 16\,000$ K with $\log n_{\rm e} \sim 2.5$ cm^{-3} and with low, but fairly typical, PN abundances. We discuss possible histories for K 1-2 and the jets. However, there are still many unknowns in the study of accretion and jet formation for such PN binary central stars.

Key words: binaries: close – binaries: spectroscopic – stars: individual: VW Pyx – stars: low-mass, brown dwarfs – planetary nebulae: individual: K 1-2.

1 INTRODUCTION

A binary nature to the central stars in planetary nebulae (PNe) is often invoked to explain the asymmetries therein. This is due, in part, to the relative ease with which the ejected common envelope (CE) is channelled naturally into the orbital plane of the binary (Iben & Livio 1993; Iben & Tutukov 1993). The resultant density contrast between the polar and equatorial regions aids break-out of the hot star's later energetic wind through the lower-density polar regions. In a survey of the morphologies of PNe with binary central stars, Bond & Livio (1990) found that in all but one case the surrounding nebulae have a non-spherical appearance. The exception is the almost perfect ring nebula, Sp 1, which Bond & Livio suggest is actually a bipolar nebula viewed nearly end-on. Further support for this model comes from Pollacco & Bell (1997), who obtained extremely deep imaging of the only known *totally* eclipsing (hence $i \sim 90^\circ$) central star, UU Sge, which has a highly collimated tube-like nebula with aspect ratio about 7:1. Recent simulations of the effect of magnetic fields in evolved single stars (Garcia-Segura, Langer & Rozyczka 1999) have rekindled the debate between single or binary star shaping models, but it is likely that binarity plays an important role in shaping, either directly through the CE phase or through the spin-up of the secondary (thus inducing the necessary magnetic fields).

The central star of the old PN K 1-2 was discovered by Bond & Grauer (1987) and displays a large-amplitude sinusoidal light-curve variation indicative of the reflection effect. The phasing of the light variations indicates that maximum brightness is situated at or near the substellar point of the secondary. While there is little doubt that the dominant process occurring is the simple reflection effect, emission lines in the spectra phase-locked to the secondary indicate that there is substantial reprocessing of the intense radiation field of the primary component adding to the light output. Ferguson & James (1994) investigated this phenomenon in the binary BE UMa. While they failed to reproduce the reprocessed emission-line spectrum in detail, their photoionization model could reproduce the continuum variations.

K 1-2 and VW Pyx were studied by Kohoutek & Schur (1982). Based on the distance (an average from various distance relations) and a $T_{\rm eff}$–luminosity–nebular line flux relation, they obtain $T_{\rm eff}$ of about 85 000 K, which would explain the high excitation class ($\geqslant$10) of the nebula.

Lutz & Lame (1989) first described the existence of 'jet-like'[1] features centrally located in the core of K 1-2. Further images were presented by Bond & Livio (1990), and the latest by Corradi et al. (1999), who also presented high-resolution spectroscopy of the jets. In general, they find little difference between the velocities of the jets and the old nebula – a result that casts doubt on the jets being an independent ejection episode. Using simple assumptions (e.g. a spherical geometry), Corradi et al. found that the jets are inclined to the line of sight by $\sim 40^\circ$, implying a binary orbital inclination, $i = 50^\circ$, *if* the jets are aligned by the binary system. This is our assumption in the analysis that follows, but we stress that we do not know this for a fact.

In this paper, we present new spectroscopic data of K 1-2 and the jets which we use to derive abundances. We also present intermediate-resolution phase-resolved spectroscopy, which, with

★E-mail: k.exter@qub.ac.uk

[1] For convenience we will refer to these as jets, although some features of jets, such as high outflow velocities, do not seem to apply.

new *BVI* photometry of VW Pyx, is used to constrain the nature of the binary components.

2 OBSERVATIONS AND DATA REDUCTION

2.1 Photometry

Imaging observations were made with the 1.0-m telescope at SAAO, on the nights of 1995 February 7–12 using Cousins *BVI* filters in photometric conditions. A Tektronix 564 × 564 pixel detector was used. Flat-field images were obtained on the twilight sky, and the seeing varied from ∼1 to 4 arcsec.

The data were reduced using scripts available within IRAF. The data reduction was limited to bias subtraction and flat-fielding corrections. Instrumental magnitudes were measured using the APPHOT package using three comparison stars and VW Pyx. All the stars measured were isolated and had signal-to-noise ration S/N > 100 in their profiles (VW Pyx was the faintest).

2.2 Long-slit spectra

Low-resolution spectroscopy was obtained with the 3.9-m Anglo-Australian Telescope in New South Wales, Australia, on the night of 1995 January 6. The RGO spectrograph was used with the 25-cm camera, 250B grating and Tektronix 1024 × 1024 pixel detector. This setup resulted in a dispersion of ∼150 Å mm^{-1} giving a nominal resolution on the detector of ∼7.5 Å. The detector was binned by a factor of 2 in the spatial direction and we imaged over the length of the slit (3 arcmin). Wavelength calibration was achieved by obtaining observations of an argon source with the same instrumental setup. Observations of a tungsten source were obtained in the afternoon before observing for flat-field purposes, and of the twilight sky to correct for variations in the slit transmission. The night was affected intermittently by fog but was photometric during the period during which these observations were taken.

The observations of K 1-2 were centred on VW Pyx and obtained at PA 155° and 90°. PA 155° contains the jet, while the other orientation samples the old PN. Aligned to the star with a slit width of 2 arcsec, the observations are not centred on, but do sample, most of the brightest parts of the jets (see Fig. 2). Two integrations of 1200 s were obtained in each PA along with short, wide-slit observations of the spectrophotometric standard star BD +08 2015 for relative flux calibration purposes.

Reduction of the data used scripts available within IRAF. Briefly, the steps involved included bias subtraction (using the strips of virtual pixels attached to the image), flat-fielding with images derived from the tungsten lamp images, correction for the vignetting function (and slit variations) using the twilight sky spectroscopic images, correction for airmass extinction, and flux calibration. Sky subtraction was carried out using the sky spectrum visible along the outer third of the slit. From the resultant images, one-dimensional spectra were extracted, shown in Fig. 1. Even a cursory glance shows that there are clear differences between the jet and old PN spectra.

2.3 Radial velocity spectra

VW Pyx was observed on 1995 April 19 and 20 with the 3.5-m ESO New Technology Telescope at La Silla under remote control from Garching, Germany. The blue optimized arm of the EMMI spectrograph was used with the 1024 × 1024 pixel Tektronix cahrge-coupled device (CCD) and the 600 line mm^{-1} grating, giving a reciprocal dispersion of 37.8 Å mm^{-1} at the focal plane. A projected slit width of 1.0 arcsec and the grating set to give a central wavelength of 4555 Å^{-1} resulted in a dispersion of ∼0.9 Å pixel^{-1}. The observations were timed using the ephemeris given by Bond & Grauer (1987). Bracketed observations of a copper–argon source were obtained approximately every 30 min during the course of the observations.

The data reduction was done using the software PAMELA and MOLLY (written by Tom Marsh) and some standard Starlink packages. The procedures included bias subtraction, flat-field correction, sky subtraction, and then extraction of the target and arc spectra. The spectra were 'optimally extracted', i.e. with weights, to give the maximum signal-to-noise ratio. Nebular lines were visible on the CCD images, and were included in the sky region selection. The wavelength calibration achieved rms residuals of 0.05 Å pixel^{-1}. The spectra were then divided by a low-order fit to the continuum and binned to a consistent velocity scale.

2.4 Imaging

The EMMI was also used in imaging mode with the filters of [O III] (centred at 5011 Å, with 55 Å full width at half-maximum, FWHM) and [N II] (6588 Å, and 30 Å FWHM), and exposures of 1200 s. The images were reduced using procedures in IRAF, including bias subtraction, flat-fielding corrections and bad-pixel masking. Cosmic rays were removed using the Starlink package BCLEAN. Images are shown in Fig. 2.

3 THE IMAGES

The NTT images of the nebula presented here are deeper than those of Corradi et al. (1999) but otherwise similar. They show a typical evolved PN with multiple shell structure, and there is some indication of more emission close to the limit of detectability. The overall size of the old PN is about 3 × 1.5 arcmin, the jets each being about 30 × 2 arcsec.

In Fig. 2 we compare the [N II] (N2) image and the [O III] (O3) image by overplotting them. The sky background counts (away from the nebula) were subtracted and each then divided by the counts in the brightest part of the upper jet, that termed A in Corradi et al. (1999). The images were shifted so that all the stars around VW Pyx were aligned. The point spread function of the O3 image is about 10 per cent larger than of the N2 image. The three features in a triangle to the right of the jet axis are stars, and most of the other features were indicated by Corradi et al. (1999) to be knots. The dynamic range in the O3 image is smaller than in the N2 image. Considering the high background flux from the nebula, this is not too surprising; count levels are 0.15 in the nebula compared to 0.35 peak in the southern knots.

All of the knots, except for the faintest lying between VW Pyx and the brightest feature in the northern jet, are resolved, having FWHM of 25 to 50 per cent greater than the stars in their narrowest width (i.e., the elongated structures are obviously resolved). These unresolved knots are seen on the narrow-band [O III] 5007 Å *HST* image shown in Fig. 3. This WFPC2 image was retrieved from the *HST* archive, and we presented the calibrated science data image which has been modified only by cosmic-ray removal and binned 2 × 2.

Corradi et al. (1999) suggested that the SE knots show evidence for ionization stratification, with the [O III] emission lying closer to

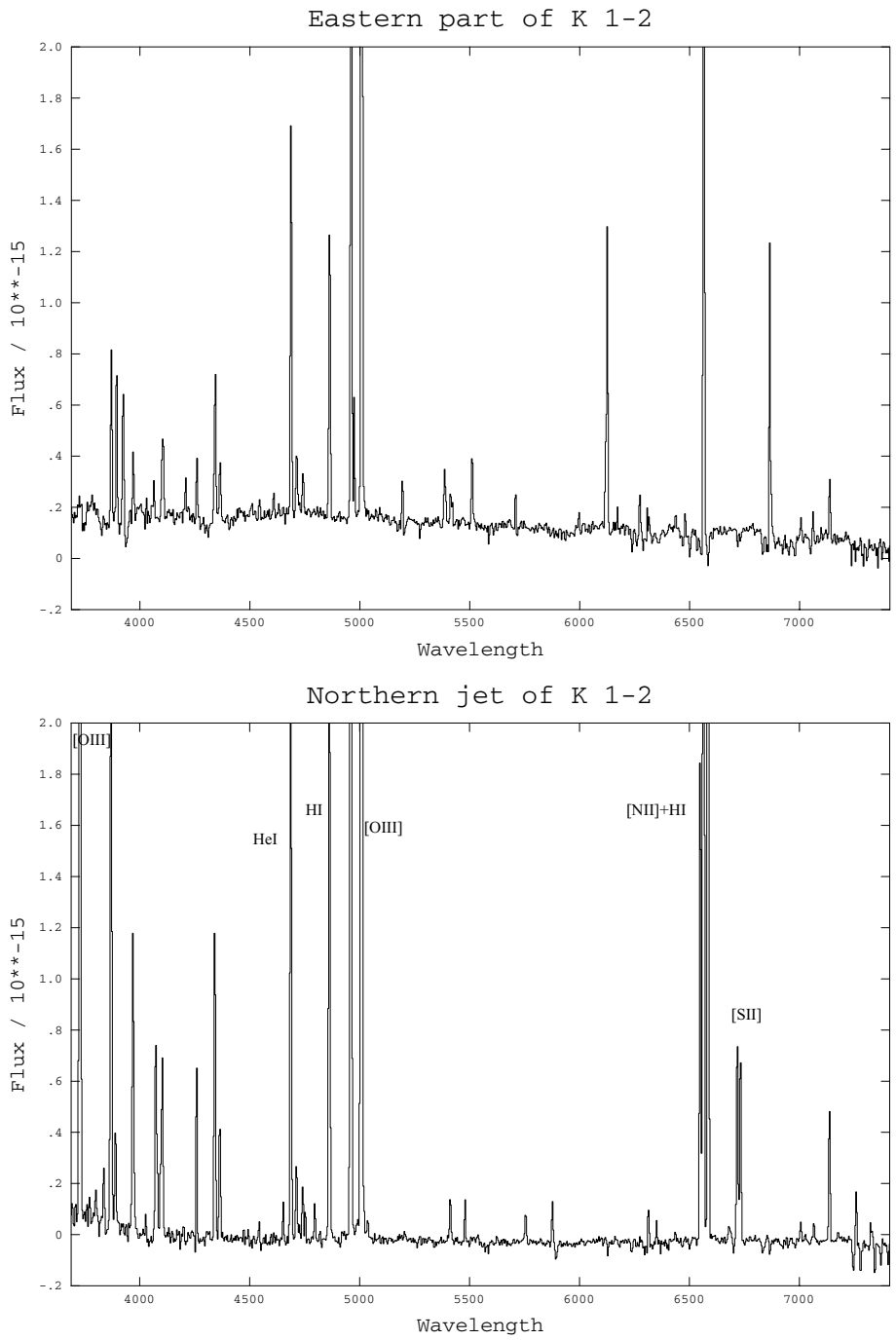

Figure 1. The dereddened spectra of the eastern part of the nebula and the northern jet of K 1-2, scaled to show the fainter lines. Emission-line identifications are given in Table 2.

the star than the [N II]. Our overlay image slightly supports this view, although better dynamic range in the O3 image would be preferred. The positions of peak brightness of the various knots shown in the contour image of Fig. 2 are within 0.4–1 pixel of each other on the O3 and N2 images. For the lowest southern knot, however, the O3 knot is 1.6 pixels (0.4 arcsec) closer to VW Pyx than the N2 knot, as measured by eye. Note, however, that both their and our filters are broad enough to contain a contribution to the flux from Hα. For our images, we estimate about 1.5 and 0.4 of the flux in the southern and northern jets, respectively.

The extended, smooth and faint feature marked A′ by Corradi et al. (1999) is visible in our N2 grey-scale image, being brighter to the north. Close inspection of the O3 grey-scale image reveals that it is also present, although fainter, and also extends in both directions.

Fig. 2 shows the structures making up the jets to be reasonably symmetrically placed within the PN. Close inspection shows that the central star is not actually positioned on the bisector between the jets, as noted by Corradi et al. (1999). The difference is not great, with a perpendicular distance of $\sim$1 arcsec to the line joining the outermost nebulous structures. There is no recorded value for

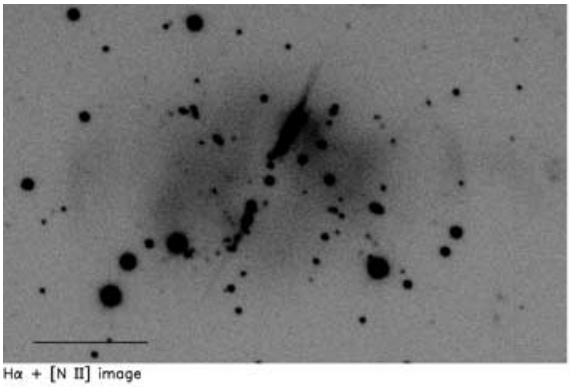

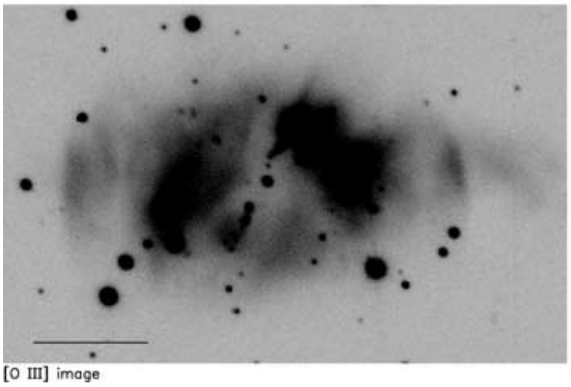

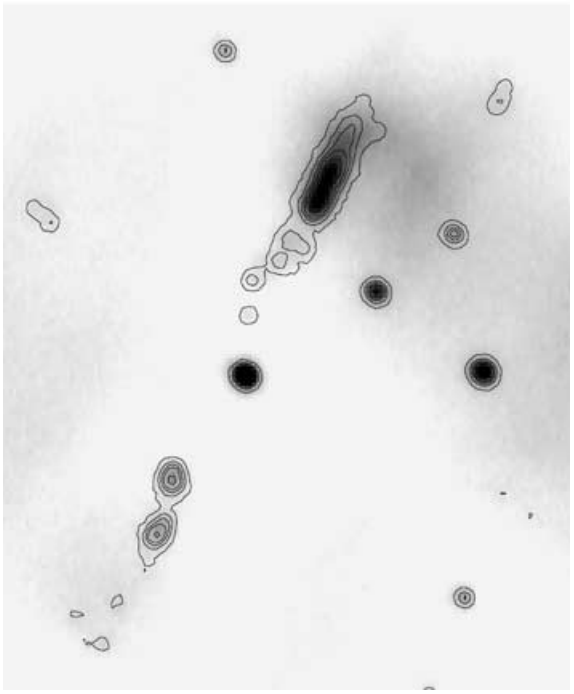

Figure 2. Top: [N II] image of K 1-2, showing the structures making up the jets. Note that the central star does not lie at the intersection of the jets. The bar, lower left, is 30 arcsec long. North is straight up and east to the left. Middle: [O III] image demonstrating the higher emission in the nebula relative to that in the jet. Several shells of emission are visible. Bottom: Overlay image, showing in grey-scale the [O III] and in contour the [N II] image. Contours are scaled 0.1, 0.2, 0.3, 0.4, 0.6, 0.8, 1.0, where 1.0 is the brightest part of the knot to the north, and the grey-scale goes from 0.1–0.9 (lower maximum value to bring out the faint emission).

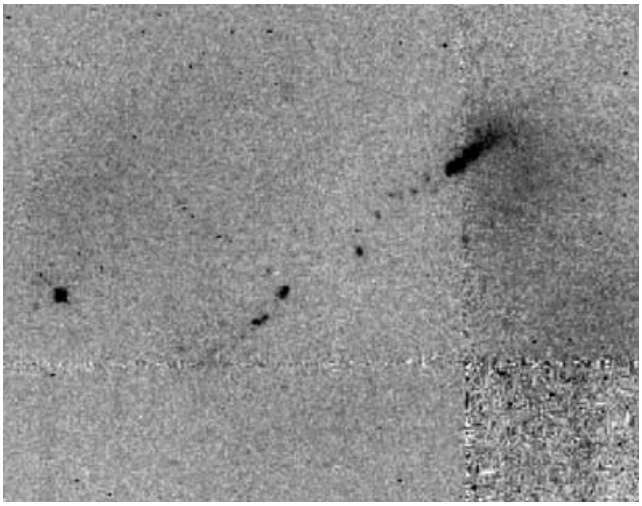

Figure 3. *HST* narrow-band [O III] image, with similar orientation and scale to the NTT images (the same features are seen on the contour image of Fig. 2).

the proper motion of VW Pyx; however, the 1979 UK Schmidt blue plate (accessed from the superCOSMOS Sky Survey website) shows likewise that the star is not quite aligned with the out-streaming structures. There is no distance recorded for VW Pyx, and hence no age for the outflows, and thus limiting stellar proper motion, can be estimated.

A possible mirror symmetry for the knots is obvious from the images of Fig. 2. However, looking closely at the topmost figure, one can see a faint feature located almost directly to the south of the central star, not visible on the other images because of its faintness. One could suppose this to be a counterpart of the closer, directly northern faint knot. Then, combined with the placement of the other knots, this could suggest a geometry formed by a rotating outflow; a multi-axial geometry with one almost north–south alignment, the other with the brightest knots. However, velocity information at minimum would be required to confirm this speculation.

One should not forget that, as Corradi et al. (1999) pointed out, there are also knots placed in a direction perpendicular to the main flow. They collected no velocity information on these. Our images show the knotty nature of the jet near the star as well as the curvature of the jets in this region. Less extreme examples of this phenomenon are found in other objects (e.g. NGC 7662, Balick 1993). In some cases this is due to collisional excitation of the emission lines by shocks with velocities of 50–80 km s^{-1}. Corradi et al. (1999) found a velocity of just 25 to 40 km s^{-1} (increasing outwards) for the K 1-2 jets, similar to that of the old PN. It is also clear, from inspecting the images and from the velocity analysis of Corradi et al. (1999), that the knots in the two jets do not match up with each other – there does not seem to be a counterpart for the southern jet, with the same distance from and angle with respect to the central star, in the northern jet.

Given we know that the central star of K 1-2 is a binary, it is reasonable to suppose that this has shaped the nebula and has something to do with the jets. It is generally accepted that an extremely tightly collimated flow must originate in an accretion disc formed around the hot component in a binary system. The most likely formation mechanism is the Roche lobe overflow (RLOF) of one of the components. Depending on the epoch at which the disc is produced,

several mechanisms are possible. These are discussed by Soker & Livio (1994), one of which may be applicable to K 1-2. The case for disc formation prior to the PN stage (taken from Pastetter & Ritter 1989) is enticing, as it would allow both for the formation of knotty jets (via spasmodic mass transfer) and for the jets to be larger in extent than the nebula, both of which are found for K 1-2. However, the models of Pastetter & Ritter predict that very long-period (years) systems would result from this situation, which does not apply to VW Pyx. Soker & Livio discuss the case for post-PN disc formation. Rough calculations of the secondary orbital shrinkage during the final stages of the CE phase suggest that the orbital decay occurs in a short period, of the order of $\geqslant$20 yr. Hence, the entropy profile in the secondary remains frozen as the mass loss is essentially adiabatic. If the secondary is fully convective or has deep convective layers, then accretion of this material can lead to substantial expansion (Prialnik & Livio 1985), and if the orbital separation is sufficiently small, mass transfer via RLOF can be initiated and a disc produced. While the jet morphology and kinematics of K 1-2 indicate that production of the jets and knots have continued throughout the PN or CE ejection phase, the apparent mass of the secondary would allow a convective envelope to form; if $M_1 = 0.5\,\mathrm{M}_\odot$ then $M_2 > 0.5\,\mathrm{M}_\odot$ (see Section 6). For a star of this mass, the Roche radius is only 30 per cent larger than the main-sequence radius.

Note, however, that it is not proven that the formation of a disc will necessarily lead to the ejection of highly collimated jets, let alone knotty ones with a 'bent' shape as found for K 1-2. Also, the modelling of accretion disc and jet formation in binaries is still a field in flux. Reyes-Ruiz & López (1999) also study the conditions under which accretion discs will form around binary systems. They find that, for a typical primary core mass of 0.6 $\mathrm{M}_\odot$ and nebular mass of 2–3 $\mathrm{M}_\odot$, RLOF will only occur when the orbital separation is $<2\,\mathrm{R}_\odot$, and subsequent mass transfer from a secondary with $M_2 > 0.08\,\mathrm{M}_\odot$ does *not* lead to a disc formation. Gonçalves, Corradi & Mampaso (2001) consider a variety of models designed to explain PNe with low-ionization structures (LIS) – jets, jet-like structures, or knots. These LIS appear in all morphological groups of PNe, and the models to explain them are generally of two types: those considering accretion disc collimated winds and those with hydrodynamic or magnetohydrodynamic winds. They conclude that these models are unable to account simultaneously for the several key characteristics of high-velocity jets, and the low-velocity jet-like structures, such as found in K 1-2, cannot be explained by any of the existing models. Lopez (1997) reviewed the formation of bipolar, rotating, episodic jets (BRETs) and other flows, and in each case the flow velocity is always significantly greater than the nebular expansion velocity. However, we cannot rule out a low-velocity collimated flow in VW Pyx, or even a higher-velocity flow if the geometry is more complex than modelled by Corradi et al. (1999). Note also that in K 1-2 there is a system of knots that appear (on the plane of the sky) to be perpendicular to the main jets (see also Corradi et al. 1999).

As Figs 2 and 3 show, the inner parts of the jets are composed of a number of resolved knots indicative of episodic mass loss, and the parts of the jet furthest from the star have a smoother appearance. The curvature of the jets or knots in the inner regions is reflectively symmetric, not point symmetric, and VW Pyx does not lie at the intersection of these regions. Soker & Rappaport (2001) studied symmetries in PN and found that binary companions in wide or close *eccentric* orbits can produce similar effects. Although the data here cannot absolutely rule out an eccentric orbit, for systems having gone through the CE phase, the close proximity of the two stars will rapidly circularize the orbit (e.g. Habets & Zwaan 1989). The curved jets may, in fact, reveal details of the history of orbital decay during the CE phase itself.

4 THE SPECTRUM OF VW PYX

The spectrum of VW Pyx contains a mixture of emission from the irradiated face of the cool secondary star, and barley visible absorption at He II from the hot primary star. Twenty spectra spread out over phase were available, and the radial-velocity-corrected sum of the best spectra is shown in Fig. 4. The two absorption lines at the end of the spectrum are the oversubtracted [O III] 4595,5007 Å nebular lines; having an uneven spatial distribution, this could not be avoided. A few other faint nebular lines were present on the CCD image, but they were well subtracted from the stellar spectrum. Table 1 lists the lines present on the spectra and their likely identifications. The spectrum is similar to that seen in the post-common-envelope binaries (PCEBs) EC 11575−1845 and V664 Cas (Acker & Stenholm 1990; Chen et al. 1995; Exter et al., in preparation).

In the stellar spectrum, the H I profiles are wide and show absorption lines at the peak. The absorption is deeper at Hβ than at Hδ. This behaviour, as well as the range of emission lines present, is qualitatively very similar to the other PCEBs mentioned above.

These profiles suggest that the most strongly irradiated regions of these stars are optically thick to light at these wavelengths: it may be here that the lines are mimicking the H-absorption spectrum of a hotter star. The breadth of the profiles, as in other PCEBs, suggests Stark broadening.

The FWHM of the emission does not vary over the orbit, and around phase 0, when the cool side of the secondary is facing us, the lines are the faintest but never quite disappear. All lines are resolved, and as measured from the averaged spectrum of Fig. 4 the FWHM of the various narrow lines is about 3 Å ($\sim$200 km s^{-1}), and for the H I lines about 10 Å ($\sim$680 km s^{-1}). This large width for the hydrogen lines is similar to that seen in EC 11575−1845 and V664 Cas, but the narrow lines are wider in VW Pyx than in these counterparts.

The spectrum of the primary star is barely visible. Looking carefully at our whole sequence of spectra, and forearmed with the knowledge gained from our work on EC 11575−1845 and V664 Cas, we believe that photospheric absorption at He II 4686 Å can just be seen underneath the emission line from the secondary star.

5 RADIAL VELOCITIES

A Gaussian fitting routine in MOLLY was used to determine the radial velocities (corrected to the heliocentric frame) of the brightest narrow lines. Because of low resolution and low signal-to-noise ratio, absolute wavelength (and thus ion) identifications are not possible (except for He II and H I). For the fits, the FWHM, height and radial velocity were usually all free parameters, with χ^2 minimization to find the best fit.

The radial velocities were then fitted with a sine curve (Fig. 5) – therefore assuming a circular orbit – using the period, P, determined from the light curve (see Section 7), to determine the time of minimum brightness, T_0, semi-amplitude, $4K$, and, for lines with certain wavelength identification, the systemic velocity, γ. To improve the final orbital solution, the radial velocities of the brightest two lines, He II 4686 Å and one at 4641 Å, were shifted to zero systemic velocity and fitted together; this resulted in $K = 93 \pm 5$ km s^{-1}. From He II we additionally find $\gamma = 70 \pm 4$ km s^{-1}. This agrees with the value of 66 ± 4 km s^{-1} derived by Kohoutek &

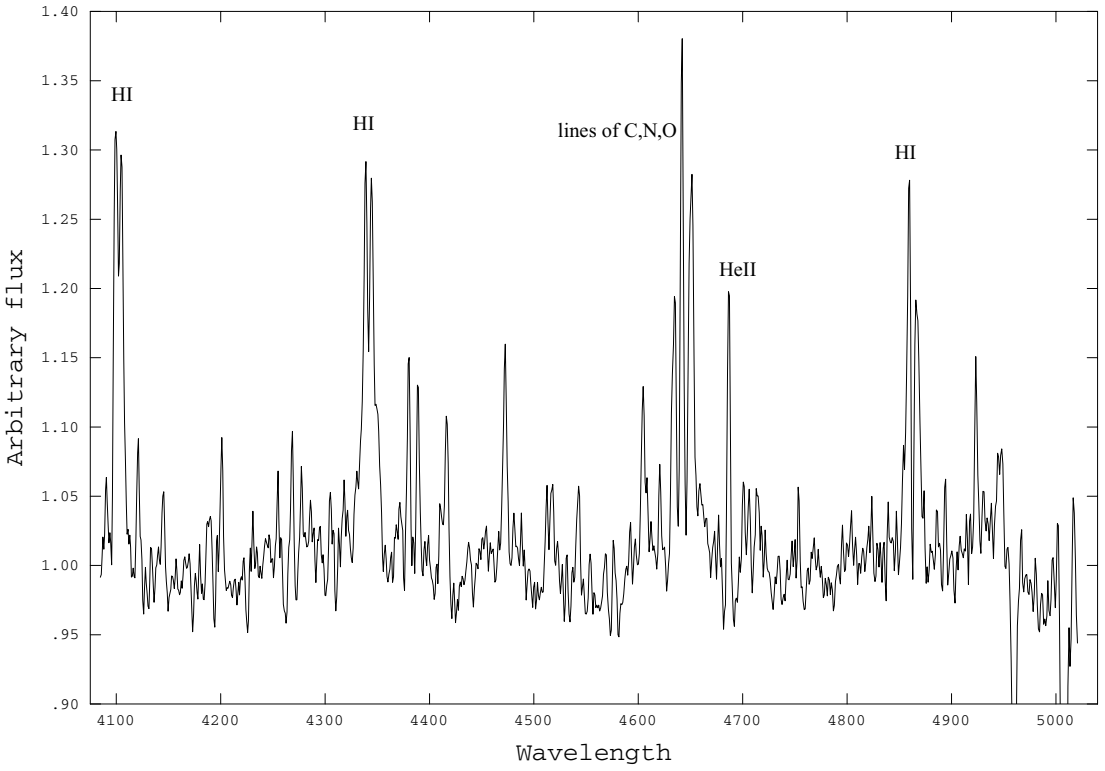

Figure 4. Radial-velocity-corrected and average spectrum of VW Pyx. Absorption lines at the end are oversubtracted nebular emission. Line identifications are given in Table 1.

Table 1. The central wavelengths and likely ion identifications from the spectrum of the binary system VW Pyx [identifications from Ferguson & James (1994)].

4088	N II, O II, O III	4517	C III
4101	Hδ	4541	He II
4120	O II, He I	4552	N II, N III
4144	N III, C III, C II, He I, N II	4567	N II
4188	N II	4575	O III
4200	O III	4591	N II, O II, Cl III
4229	N II, C IV	4603	N II, O II, Cl III
4253	N II, C III	4619	N II
4268	C II	4633	N II, N III
4276	N II, O II	4640	C II, N III, O II
4285	N II, O II	4650	C III, O II
4303	N II	4675	C III, O II
4317	O II, C III	4686	He II
4341	Hγ	4700	N II, O II
4379	C III	4705	N II
4388	He I, C III	4713	He I
4408	O II	4752	O II
4414	O II	4862	Hβ, N III
4471	He I	4884	N II, N III
4479	Mg II, Al III	4892	N II, C III
4486	O II	4922	O II
4511	N II, O III	4945	O II

Schur (1982), using nebular spectra taken in two slit positions. We find $T_0 = 244\ 9756.51(1)$ – agreeably close to the value derived from the light curve, given the sparse distribution of radial velocity data.

For H I, one or two Gaussian profiles were required to fit the emission lines (fixed to be of the same radial velocity), and one to

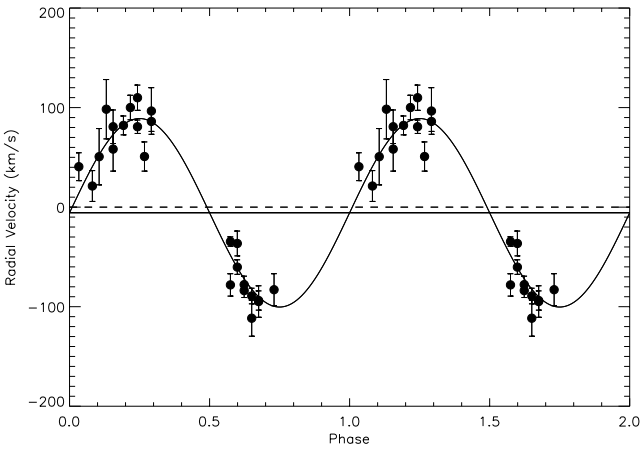

Figure 5. Radial velocity curve and sine fit from He II 4686 Å and the blend near 4641 Å.

fit the absorption line (allowed its own radial velocity). The most reliable sine fit is obtained by combining the emission and absorption radial velocities (fitted separately, they show the same γ and K values) for Hδ, resulting in $K = 86 \pm 7$ km s^{-1}, with $\gamma = 45$ km s^{-1} if not fixed to that derived above.

The value of $\sim$93 km s^{-1} for $K_{\rm em}$, the semi-amplitude of the emission lines that arise from the heated surface, provides a lower limit to the value of K for the centre of mass of the secondary star itself (the irradiated face is closer to the centre of mass of the system and so will have a smaller K value). The mass function for a single-lined binary is

$$f(m) = 1.0361 \times 10^{-7} K_2^3 P = M_1^3 \sin^3 i/(M_1 + M_2)^2,$$

where $M_{1,2}$ are the masses of the primary and secondary stars, and all units are in solar masses, days and km s^{-1}. Using $K_{\rm em}$ in place of K_2 (and bearing in mind $K_{\rm em} < K_2$), we obtain $f(m) > 0.056$. Assuming a mass for the primary of 0.6 $M_\odot$ (an average white dwarf mass) and $i = 50^\circ$, $M_2 > 0.74$ $M_\odot$. For $M_1 = 0.4$ $M_\odot$, $M_2 > 0.33$ $M_\odot$; and for $M_1 = 1$ $M_\odot$, $M_2 > 1.97$ $M_\odot$. The lower limit to the semimajor axis, a_2, for the secondary star, $(0.019\,758\ K_2 P)/\sin i$, is 1.6 $R_\odot$.

6 MASSES

At $M_1 \geqslant 0.5$ $M_\odot$ (for an assumed inclination of 50°), the secondary star of VW Pyx is the more massive, >0.5 $M_\odot$; this is possibly also the case for $M_1 < 0.5$ $M_\odot$, depending on the difference between K_2 and $K_{\rm em}$. While this could suggest that the secondary is a white dwarf, light-curve analysis and the rich emission-line spectrum would seem to rule this out. Furthermore, there are no indications of the (cool side of the) secondary's photospheric spectra in our data, thereby ruling out a giant, so the secondary is likely to be a low- or intermediate-mass main-sequence object.

Although the number of PCEBs with mass ratio determinations is small, we can say that VW Pyx would be unusual as a short-period system if indeed $q < 1$. In a compilation of PCEBs (Barman 2002, adapted from Hillwig, Honeycutt & Robertson 2000), about 10 out of the 30 have $q \leqslant 1$, only five of which have $P < 1$ d, and only two of which are similar to VW Pyx, consisting of a degenerate plus main-sequence star with period of ∼0.5 d. Of the PN central stars with $q < 1$ on the list, V651 Mon ($q \sim 0.2$) has a long period (16 d), and MT Ser ($q \sim 1$, $P = 2.7$ h) has poorly derived masses and may even be a doubly degenerate system [adopting the results of Bruch, Vaz & Diaz (2001) rather than those listed in Barman (2002)]. Not on Barman's list, V664 Cas (Exter et al., in preparation), $P = 14$ h, also has a mass ratio ∼1. Compared to the mass distributions for the non-doubly degenerate objects in Barman's list (M_1 versus M_2 or versus q), VW Pyx sits on the edge, but, for all except the highest M_1 possibilities, is part of the overall distribution. However, very small mass ratios are more common among long-period systems and those of a different PCEB type to VW Pyx. This could in part be due to selection effects; most of the objects in Barman's compilation seem to have been found serendipitously, because of unusual colours, the presence of emission lines (from the irradiated face) or light curve variations.

If VW Pyx is to have a typical mass ratio, the mass of the primary star would need to be low, <0.5 $M_\odot$. Less than about 0.3–0.4 $M_\odot$, the primary would not get hot enough within the lifetime of the nebula (a few times 10^4 yr) to excite the hydrogen (Iben & Livio 1993; Yungelson, Tutukov & Livio 1994). Less than about 0.4 $M_\odot$ (e.g., see the binary evolution models of Iben & Livio 1993), the star would not reach a $T_{\rm eff}$ of 85 000 K (Kohoutek & Schur 1982), although this temperature is not based on spectral fitting and so will be uncertain. According to Iben & Tutukov (1986), a low-mass (by which we mean 0.3–0.4 $M_\odot$, to compare to the possibilities for VW Pyx) CO or CO + He remnant will be produced from a component of initial mass <3 $M_\odot$ which experiences a case-B Roche lobe overflow event. A far larger number of the low-mass white dwarfs will be of pure He composition, and although these stars can be as massive as 0.5 $M_\odot$, their average mass, 0.25 $M_\odot$, makes it a less likely possibility for the primary star of VW Pyx. Another PN central star with a low-mass primary is V651 Mon. Its mass is is thought to be 0.4 $M_\odot$, and it is suggested (Iben & Livio 1993) that the two components initially had similar masses, about 1.8 $M_\odot$ (although the very different period of V651 Mon means that it is probably not a sister to VW Pyx).

Of the model predictions of the distribution of parameters of binary systems, evolved from an initial distribution of parameters, it is not rare to find systems with $q < 1$ (e.g. Han, Podsiadlowski & Eggleton 1995), although we are not aware of any analytical study predicting the relationship between q and period for systems similar to VW Pyx to which we could compare. Unfortunately, the understanding of various details of the CE phase – such as when it ends – and knowledge of the initial distribution of binary parameters is not complete. Hence, we cannot draw any definitive conclusions on the possible evolutionary history of VW Pyx.

Finally, one should consider whether it is possible that the secondary star of VW Pyx gained any mass during the CE phase, thus leading to a reversal of the mass ratio. It is not normally considered to occur, although the response of the secondary star to the CE phase is less well studied than that of the primary star. Hjellming & Taam (1991) look at the situation for a 1.25 $M_\odot$ secondary star within the envelope of its asymptotic giant branch companion. Initially the star does accrete material, but later fills its Roche lobe and transfers most of the material back to the primary. Soker & Livio (1994), however, point out that these calculations imply that the secondary star is far from thermal equilibrium when it emerges from the CE. These final stages of the CE phase are very short, and hence RLOF from the secondary to the primary may occur. Iben & Tutukov (1986) mention a possible scenario involving two components of initially similar mass which experience case-B mass transfer in the first instance, in which the secondary may accrete considerable mass, eventually producing a larger-mass degenerate dwarf than the primary.

7 LIGHT CURVE

The differential magnitudes of VW Pyx with respect to three comparison stars were calculated for the V-, B- and I-band data. The differential magnitudes formed between the comparison stars are flat, with a scatter of ±0.03 mag. The V-band data of VW Pyx were fitted with a double cosine curve (with the minimum brightness at $\Phi = 0$) using least-squares minimization, mimicking a reflection plus an ellipsoidal variation,

$$A + B\cos\theta + C\cos 2\theta,$$

where B is the flux semi-amplitude, A is the mean value, and C/A is ∼4 per cent (phased data shown in Fig. 6), producing the ephemeris

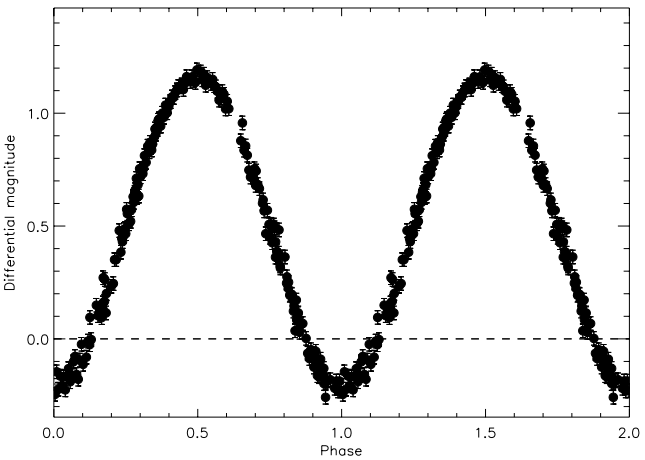

Figure 6. V-band light curve for VW Pyx. Minimum brightness is at $\Phi = 0$.

T_0(HJD) = 244 9756.466(1) + 0.6758(3) E. The *B*- and *I*-band data consist of only a dozen or so data points each, and these fit well to the same ephemeris. No corrections were made for colour and airmass effects.

Tests using LIGHT2 (Hill 1987) indicated that the light curve of VW Pyx can be modelled by a primary component somewhat larger than a white dwarf with $M \sim 0.5$ M$_\odot$, and a near-main-sequence secondary component of 0.7 M$_\odot$. Adoption of a physically unrealistic heating efficiency for the secondary is necessary to match the amplitude of the light curve. The use of the heating efficiency to model the reflections effect is described in the analysis of UU Sge (Pollacco & Bell 1993; Bell, Pollacco & Hilditch 1994) and V477 Lyr (Pollacco & Bell 1994). It should also be noted that the model used within LIGHT2 could not reproduce the full sinusoidal nature of the light curve of VW Pyx, indicating that the temperature profile of the heated area of the secondary may be more complicated than the model within LIGHT2 can generate. None the less, temperatures on the secondary component may well exceed 40 000 K at the substellar point. These results demonstrate clearly the need for an additional source of heating and serve to reinforce the conclusions of Ferguson & James (1994) that reprocessing of the primary's intense radiation field would add substantially to the continuum flux. We would here direct you to the work of Barman (2002), who modelled the atmospheres of and spectra expected from irradiated binaries. He finds that, even for lower-temperature counterparts to VW Pyx, the upper atmosphere of the secondary star suffers a considerable temperature inversion as a result of the irradiation, and moreover that the spectra seen will vary with orbital phase and inclination.

8 THE NEBULA K 1-2

From the images of Fig. 2 it is apparent that the spectra taken along the jets will be contaminated by emission from the surrounding nebula. We have not attempted to correct for this. Our raw spectra show $F(\mathrm{H}\beta)$ fluxes of 7.5, 7.5, 6.6 and 10×10^{-15} erg s^{-1} cm^{-2} for the nebula east, nebula west, jet south and jet north spectra (note that the spectra are from narrow-slit observations). On the Corradi et al. (1999) images the Hβ and Hα surface brightness distributions are smooth. Taking into account that the jet is approximately three-quarters as long as the nebula, this means that, of the flux from the jet north spectrum, 50 per cent is nebular contamination, and for the jet south spectrum, 80 per cent. However, we cannot be sure that this applies to all ions. The [O III] nebular surface brightness distribution is not uniform and there is no [N II] nebular emission. Indeed, we find 20 per cent *less* [O III] flux in the jet south spectrum compared to the nebula, but about 60 per cent more in the jet north spectrum. Moreover, it is not clear from the images whether the bow-shaped emission feature in the north is from the nebula or the jet; arguing for a symmetrical nebula, it is more likely to be from the latter.

The spectra were dereddened using the value of $c(\mathrm{H}\beta)$ derived from the ratio of the measured fluxes Hα/Hβ to the theoretically predicted values for a nebula at electron temperature $T_\mathrm{e} = 10^4$ K, electron density $n_\mathrm{e} = 10^4$ cm^{-3} (Hummer & Storey 1987) under case-B conditions of recombination relative to H$^+$ (Osterbrock 1989).[2] We used the reddening law of Howarth (1983) and $R = 3.1$. We find $c(\mathrm{H}\beta) = 0.28$ for the jet spectra and 0.11 for the nebula spectra [quite different from the value of 0.77 from Cahn & Kaler (1971), based, however, on a rather long chain of reasoning]. Nebular line fluxes were measured via Gaussian profile fitting with ELF in the Starlink package DIPSO, and the dereddened values ratioed to that of Hβ are presented in Table 2. Note that, if there is the same amount of contamination of the jet spectra by the nebula at Hβ and Hα, the calculation of $c(\mathrm{H}\beta)$ will not be affected.

There are differences between the jet north and jet south spectra, as can be seen from the entries of Table 2, which we do not find between the two nebula spectra (although for these there are unidentified lines present in one but not the other). Differences are in fact to be found for most of the measured lines. Particularly striking are the much stronger lines of [O III], [N II] and [S II], and to a lesser degree He I 5876 Å, in the jet north spectrum compared to the jet south, which in turn is somewhat weaker in the He II lines. An extremely large difference is also found for the flux of He I + [Ne IV] + H I 3889 Å, where the ratio of jet south to jet north is 11; most of the difference is probably due to the helium and/or neon line, as the other H I lines are fairly similar to each other. These differences imply different conditions in the various jet features, which would prove interesting for further study.

VW Pyx was observed with the *IUE* satellite on 1985 January 27 with the large aperture, exposure SWP24987, extracted as a point source. The only visible emission line is that of He II 1640 Å, which could come from the nebula or the irradiated secondary star.

8.1 Abundances

The spectra of the nebula and jet of K 1-2 were analysed for their abundances. The electron temperature (T_e) values were calculated using the ratios [O III] 4959+5007/4363 Å (for T_O) and [N II] 6548+6584/5755 Å (for T_N), and electron density (n_e) is calculated from the ratio [S II] 6717/6731 Å. This latter is best used for lower-density nebulae, and thus may not be the best measure of the density in the centre of the knots, if one assumes the surface brightness profile measures the density profile. The [Ar IV] 4711/4740 Å ratio (normally best used for high-density nebulae) is below the low-density limit. For these and the following calculations, the line ratios from both nebular spectra were averaged to produce one set. The T_N for the jet was calculated from the north line ratios, as the errors are much lower. When available, both T_e were used, that from the [N II] ratio for the doubly and lower ionized species. The programs EQUIB and RATIO (written by I. D. Howarth and S. Adams) were used to solve the equations of statistical equilibrium to obtain the n_e and T_e values. The atomic data used in the diagnostic and abundance analyses are referenced in Table 3.

For the southern jet we find $T_\mathrm{O} = 16\,500 \pm 2000$ K, $T_\mathrm{N} = 11\,000 \pm 1000$ K and $\log n_\mathrm{e} = 2.6 \pm 0.3$ cm^{-3}. For the northern jet $T_\mathrm{O} = 15\,600 \pm 2000$ K, while T_N and n_e are the same as for the southern jet. For the nebula we find $T_\mathrm{O} = 17\,500 \pm 1000$ K for an assumed $\log n_\mathrm{e} = 2.7 \pm 0.3$ cm^{-3} (the value decreases by only 500 K for a more normal $\log n_\mathrm{e} = 4$ cm^{-3}). Note that, as long as any nebular contamination in the [O III] line is the same at the long and short wavelengths, the value of T_O will not change.

The abundances for the collisionally excited lines were calculated using EQUIB and are given in Table 4. For the helium abundance we did not include that from 7065 Å as it is affected by a collisional contribution to the flux. For the other helium lines we employed the corrections of Clegg (1987), as written in a program by X. Liu (UCL). Helium ionic abundances are derived assuming case-B recombination relative to H$^+$ (Osterbrock 1989). The abundance of

[2] As the nebula is of very high excitation and likely to be optically thin to the H^0 and He^0 continua, case-A conditions would apply. However, the Hα flux ratio is little different between the two cases.

Table 2. The measured, dereddened line fluxes for the spectra taken of the northern and southern parts of the jet and eastern and western parts of the nebula. Errors are given in parentheses, and fluxes are ratioed to that of Hβ = 100. Ions are given for those identified. Label 'pp' means possibly present.

	Nebula west	Nebula east	Jet south	Jet north		Nebula west	Nebula east	Jet south	Jet north
[O II] 3727	14(3)		71(4)	181(5)	[O III] 5007	759(19)	697(24)	504(23)	806(37)
3760			65(4)		5082	51(2)			
H I 3798				6(1)	[N I] 5200				1(1)
H I 3835			10(2)	9(1)	5261	12(1)			
3847	90(4)				5388	16(1)	18(2)		
[Ne III] 3868	58(4)	54(8)	52(3)	104(5)	He II 5411	10(1)	10(2)	7(1)	6(1)
3880			55(3)		5439	6(1)			
He I, H I 3889	31(3)		176(10)	16(1)	5479				5(1)
3894		45(7)			5510		24(2)		
3923		41(15)			5631			7(1)	
H I, [Ne III] 3968	51(4)	20(4)	30(3)	49(3)	5707		11(2)		
4012 [Ne III], C III?	50(3)				[N II] 5755			3(3)	4(1)
He I 4026				2(1)	He I 5876			3(1)	5(1)
[S II] 4073				37(2)	5967	6(1)			
H I 4101		33(5)	26(3)	35(2)	6018			23(1)	
4122			45(3)		6125		89(4)		
4207		13(8)			[S III] 6312	5(3)	pp	5(2)	5(1)
4258		17(3)		23(2)	6406	24(2)			
H I 4340	42(4)	51(3)	51(4)	46(3)	[Ar V] 6435		8(3)	4(2)	
[O III] 4363	17(3)	21(2)	12(2)	18(1)	6480	9(2)	7(3)		
4444			9(4)		[N II] 6548			29(3)	71(4)
4463	17(3)				H I 6563	285(7)	285(10)	285(14)	285(13)
4506			22(4)		[N II] 6584			84(5)	237(11)
4542	4(3)	7(4)	4(4)	3(2)	6647			10(2)	
4652				5(4)	6678				3(1)
He II 4686	122(4)	133(13)	109(7)	89(6)	6688				2(1)
[Ar IV], [Ne IV], He I 4712	21(2)	23(4)	18(4)	12(4)	[S II] 6717			10(2)	31(2)
[Ar IV] 4740	14(2)	15(5)	12(4)	8(4)	[S II] 6731			9(2)	29(2)
4766	9(2)				6894		81(4)		
4796				5(4)	[Ar V] 7005	7(2)	7(3)	7(2)	3(1)
H I 4861	100(3)	100(5)	100(6)	100(7)	He I 7065		8(3)		3(1)
4894	11(2)				[Ar III] 7135	29(3)	21(3)	13(2)	19(1)
[O III] 4959	256(7)	235(8)	185(10)	271(13)	7180	78(3)			
4974		31(3)			[O II] 7325				4(2)

Table 3. References for atomic data.

Ion	Transition probabilities	Collision strengths
O^+	Zeippen (1982)	Pradhan (1976)
O^{2+}	Nussbaumer & Storey (1981)	Aggarwal (1983)
N^+	Nussbaumer & Rusca (1979)	Stafford et al. (1994)
Ar^{2+}	Mendoza & Zeippen (1983)	Johnson & Kingston (1990)
Ar^{3+}	Mendoza & Zeippen (1982a)	Zeippen, Butler & Le Bourlot (1987)
Ar^{4+}	Mendoza & Zeippen (1982b)	Mendoza (1983)
Ne^{2+}	Mendoza (1983)	Butler & Zeippen (1994)
S^+	Mendoza & Zeipen (1982a), Keenan et al. (1993)	Keenan et al. (1996)
S^{2+}	Mendoza & Zeippen (1982b)	Mendoza (1983)

Ne^{2+} was not calculated from 4012 Å because it gave the very high value of 0.2, so the line is probably heavily contaminated, possibly by C III.

To correct for the unobserved ionic stages we employed the ionization correction factor (ICF) scheme taken from Kingsburgh & Barlow (1994), which in turn is based on detailed photoionization models for 10 PNe, by Walton, Barlow, Monk and Clegg (unpublished). The abundances of neutral species were not derived; the fractions of neutral to ionized abundances is assumed to be the same as that for hydrogen, in which case the final abundance ratios with respect to hydrogen are not affected. Unfortunately, this ICF scheme cannot be used for the derivation of the nebular abundances. The ICF scheme for very high excitation PN, where no He I is observed, requires the measurement of [Ne V] 3426 Å, which we do not have. The derivation of abundances for these highly ionized PNe, in particular, would anyway be best done with photoionization modelling. Therefore, for the nebula we derive only the ionic abundances.

The ionization states of the jet north and south are different; the former is more abundant in most ions, except He^{2+} and Ar^{3+}, Ar^{4+}, and has a different ratio of low to highly ionized ions, except for oxygen. The elemental abundances are, however, similar to each other. The nebula's abundance pattern shows a high ionization state, completely different from that for the jets; no He^+ but with He^{2+}, no S^+ but with S^{2+}, and a very low ratio of O^+/O^{2+}. Note that the spectrum of nitrogen has few representative high ionization lines in the optical and hence requires substantial correction (factor of 10) for unseen states.

Table 4. The ionic abundances of the old PN K 1-2 and the ionic and total abundances of the jets.

		Jet south	Jet north	Nebula			Jet south	Jet north	Nebula
6678	He^+/H^+		7.169e−02		3868	Ne^{2+}/H^+	1.002e−05	2.335e−05	9.871e−06
5876	He^+/H^+	2.311e−02	3.830e−02			*ICF(Ne)*	*4.29*	*2.80*	
Avg.	He^+/H^+	2.31e−02	5.50e−02			**Ne/H**	**4.30e−05**	**6.54e−05**	>9.87e−06
4686	He^{2+}/H^+	9.528e−02	7.602e−02	1.136e−01					
	He/H	**1.18e−01**	**1.31e−01**	**1.14e−01**	7135	Ar^{2+}/H^+	4.200e−07	6.737e−07	7.547e−07
					4740	Ar^{3+}/H^+	7.670e−07	5.590e−07	8.389e−07
5007	O^{2+}/H^+	4.436e−05	8.110e−05	5.953e−05	7005	Ar^{4+}/H^+	4.153e−07	1.879e−07	4.114e−07
4959	O^{2+}/H^+	4.687e−05	7.840e−05	5.786e−05		*ICF(Ar)*	*1.12*	*1.26*	
4363	O^{2+}/H^+	4.525e−05	8.352e−05	5.930e−05		**Ar/H**	**1.79e−06**	**1.78e−06**	**>2.01e−06**
Avg.	O^{2+}/H^+	4.55e−05	8.10e−05	5.89e−05					
7325	O^+/H^+		5.169e−05		6731	S^+/H^+	3.912e−07	1.219e−06	
3727	O^+/H^+	2.021e−05	4.055e−05	8.775e−07	6717	S^+/H^+	3.880e−07	1.191e−06	
Avg.	O^+/H^+	2.02e−05	4.61e−05	8.77e−07	*Avg.*	S^+/H^+	3.90e−07	1.20e−06	
	ICF(O)	*2.97*	*1.78*		6312	S^{2+}/H^+	1.877e−06	2.288e−06	1.848e−06
	O/H	**1.95e−04**	**2.27e−04**	**>5.98e−05**		*ICF(S)*	*1.53*	*1.26*	
						S/H	**3.47e−06**	**4.42e−06**	**>1.85e−06**
6584	N^+/H^+	1.164e−05	3.304e−05						
6548	N^+/H^+	1.194e−05	2.891e−05			*Logarithmic total abundances*			
5755	N^+/H^+	2.370e−05	3.275e−05			log(O/H + 12)	8.29	8.36	
Avg.	N^+/H^+	1.18e−05	3.16e−05			log(N/H + 12)	8.06	8.19	
	ICF(N)	*9.66*	*4.92*			log(Ne/H + 12)	7.63	7.82	
	N/H	**1.14e−04**	**1.55e−04**			log(Ar/H + 12)	6.25	6.25	
						log(S/H + 12)	6.54	6.65	

We compared the ratio of the low to high ionization ion abundances, for each element for the jets, to the average of the Galactic disc sample of PNe of Kingsburgh & Barlow (1994). The jets, while definitely being of lower ionization than the nebula (the comparative ratio for the oxygen ions shows that clearly), have otherwise a similar status to the disc average. However, the jets are obviously overabundant in He^{2+} compared to He^+, which is at odds with its other ionization ratios. We believe therefore that there is contamination from the old nebula of the jet spectra especially in He II. If so, the ICFs, and thus total abundances, for O and N would decrease.

Pollacco & Bell (1997) analysed four PNe thought to be ejected common envelopes and in each case found similar physical conditions, i.e. low n_e and higher than typical T_e (most from T_O). They found similar He abundances to those found here and an oxygen deficiency of 0.5 dex compared to a typical PN. In common with Abell 46 (Pollacco & Bell 1997), N is absent in the old PN. In the case of Abell 46 the conclusion was that the nebula probably really is N deficient, and the same argument could apply here (it is difficult to see how the [O II] 3727 Å line could be detected and not the [N II] 6584 Å line). For K 1-2 we find a slight O deficiency (0.4 dex) in the jets, compared to the mean disc value of 8.68. N is similarly low compared to 8.72 for the Type I disc PNe in the Kingsburgh & Barlow (1994) sample, but normal compared to 8.14 for the non-Type I PNe only (Type I PNe are thought to have evolved from higher-mass precursor stars than the non-Type I PNe). S and Ne are also slightly deficient (0.4–0.5 dex) compared to the Kingsburgh & Barlow survey results. So overall we find typical, but slightly low, abundances in the jets.

9 SUMMARY

VW Pyx is a member of the rather sparsely populated class of binary PN central stars, which shows a rich emission-line spectrum and large reflection effect as a result of the irradiation of the secondary star by the very hot primary star. VW Pyx has not been much studied in great detail, but our analysis suggests that it is potentially a very unusual object. Adoption of the inclination of the jets determined by Corradi et al. (1999) for the binary leads to a secondary mass larger than that of the primary, for a primary mass of $>0.5\ M_\odot$. We do not, however, have an independent value for the inclination of the binary system; we adopt this value because it seems reasonable that the outflow and orbital axis are the same. *If* this is correct, then in comparison with PCEBs of similar periods and stellar types, the q for VW Pyx is unusual. The nebula, K 1-2, and the jets were analysed for their line fluxes and abundances, although we make no correction for the contamination of the jet-like spectra by the nebula. We find notable differences between the line ratios (to Hβ) and ionic abundances in the jet north and jet south features, but their overall abundances are similar, being slightly deficient or normal compared to those for Galactic disc PNe. The old nebula is deficient in nitrogen and displays a high ionization state, compatible with the suggested high temperature for the primary star. The jets are broken up into individually resolved knots, and are are highly collimated and bent, showing most obviously mirror symmetry but with a possibility of multi-axial symmetry. These conditions could suggest that, at some time in the recent past, an accretion disc was present in the system.

ACKNOWLEDGMENTS

We thank Tom Marsh for the use of PAMELA and MOLLY. This work made much use of the Simbad data base, maintained by the Centre de Données astronomiques de Strasbourg, and the NASA Astrophysics Data System. Some of this work is based on observations made with the NASA/ESA *Hubble Space Telescope*, obtained from the data archive at the Space Telescope Science Institute. STScI is operated by the Association of Universities for Research in Astronomy, Inc., under NASA contract NAS 5-26555.

REFERENCES

Acker A., Stenholm B., 1990, A&A, 233, L21
Aggarwal K. M., 1983, ApJS, 52, 387

Balick B., 1993, in Weinberger R., Acker A., eds, Proc. IAU Symp. 155, Planetary Nebulae. Kluwer, Dordrecht, p. 131
Barman T. S., 2002, PhD thesis Univ. Georgia
Bell S. A., Pollacco D. L., Hilditch R. W., 1994, MNRAS, 270, 449
Bond H. E., Grauer A. D., 1987, in Philip A. G. D., Hayes D. S., Liebert J., eds, IAU Colloq. 95, Second Conference on Faint Blue Stars. L. Davis Press, Schenectady, p. 221
Bond H. E., Livio M., 1990, ApJ, 555, 568
Bruch A., Vaz L. P. R., Diaz M. P., 2001, A&A, 377, 898
Butler K., Zeippen, C. J., 1994, A&AS, 108, 1
Cahn J. H., Kaler J. B., 1971, ApJS, 22, 319
Chen A., O'Donoghue D., Stobie R. S., Kilkenny D., Roberts G., van Wyk F., 1995, MNRAS, 275, 100
Clegg R. E. S., 1987, MNRAS, 229, 31
Corradi R. L. M., Perinotto M., Villaver E., Mampaso A., Gonçalves D. R., 1999, ApJ, 523, 721
Ferguson D. H., James T. A., 1994, ApJS, 94, 723
Garcia-Segura G., Langer N., Rozyczka M., 1999, ApJ, 517, 767
Gonçalves D. R., Corradi R. L. M., Mampaso A., 2001, ApJ, 547, 302
Habets G. M. H. J., Zwaan C., 1989, A&A, 211, 56
Han Z., Podsiadlowski P., Eggleton P. P., 1995, MNRAS, 272, 800
Hill G., 1987, LIGHT2 User Manual. Internal Publication, Dominion Astrophysical Observatory
Hillwig T. C., Honeycutt R. K., Robertson J. W., 2000, ApJ, 120, 1113
Hjellming M. S., Taam R. E., 1991, ApJ, 370, 709
Howarth I. D., 1983, MNRAS, 203, 301
Hummer D. G., Storey O. J., 1987, MNRAS, 224, 801
Iben I. Jr., Livio M., 1993, PASP, 105, 1373
Iben I. Jr., Tutukov A. V., 1986, ApJ, 311, 753
Iben I. Jr., Tutukov A. V., 1993, ApJ, 418, 343
Johnson C. T., Kingston A. E., 1990, J. Phys. B, 23, 3393
Keenan F. P., Hibbert A., Conton E. S., Ojha P. C., 1993, Phys. Scr., 48, 129
Keenan F. P., Aller L. H., Bell K. L., Hyung S., McKenna F. C., Ramsbottom C. A., 1996, MNRAS, 281, 1073
Kingsburgh R. L., Barlow M. J., 1994, MNRAS, 271, 257
Lopez J. A., 1997, in Habing H. J., Lamers H. J. G. L. M., eds, Proc. IAU Symp. 180, Planetary Nebulae. Kluwer Academic, Dordrecht, p. 197
Lutz J., Lame N. J., 1989, in Torres-Peimbert S., ed., Proc. IAU Symp. 131, Planetary Nebulae. Kluwer, Dordrecht, p. 462
Kohoutek L., Schur G. F. O., 1982, MNRAS, 201, 21
Mendoza C., 1983, in Flower D. R., ed., Proc. IAU Symp. 103, Planetary Nebulae. Reidel, Dordrecht, p. 143
Mendoza C., Zeippen C. J., 1982a, MNRAS, 198, 127
Mendoza C., Zeippen C. J., 1982b, MNRAS, 199, 1025
Mendoza C., Zeippen C. J., 1983, MNRAS, 202, 981
Nussbaumer H., Rusca C., 1979, A&A, 72, 129
Nussbaumer H., Storey P. J., 1981, A&A, 99, 177
Osterbrock D. E., 1989, Astrophysics of Gaseous Nebulae and Active Galactic Nuclei. University Science Books, Mill Valley, CA, and Oxford Univ. Press, Oxford
Pastetter L., Ritter H., 1989, A&A, 214, 186
Pollacco D. L., Bell S. A., 1993, MNRAS, 262, 377
Pollacco D. L., Bell S. A., 1994, MNRAS, 267, 452
Pollacco D. L., Bell S. A., 1997, MNRAS, 284, 32
Pradhan A. K., 1976, MNRAS, 177, 31
Prialnik, D., Livio, M., 1985, MNRAS, 216, 37
Reyes-Ruiz A., López J. A., 1999, ApJ, 524, 952
Soker N., Livio, M., 1994, ApJ, 421, 219
Soker N., Rappaport S., 2001, ApJ, 557, 265
Stafford R. P., Bell K. L., Hibbert A., Wijsundera W. P., 1994, MNRAS, 268, 816
Yungelson L. R., Tutukov A. V., Livio M., 1993, ApJ, 418, 794
Zeippen C. J., 1982, MNRAS, 198, 111
Zeippen C. J., Butler K., le Bourlot J., 1987, A&A, 188, 251

This paper has been typeset from a TEX/LATEX file prepared by the author.